ISSN 2070-0504, Catalysis in Industry, 2014, Vol. 6, No. 1, pp. 44–52. © Pleiades Publishing, Ltd., 2014.
Original Russian Text © G.E. Bekmukhamedov, S.R. Egorova, A.A. Lamberov, 2013, published in Kataliz v Promyshlennosti.

DOMESTIC CATALYSTS

Effect of the Nature of Silicon Oxide Structures on the Activity of an Alumina–Chromium Catalyst in the Reaction of *iso*-Butane Dehydrogenation

G. E. Bekmukhamedov, S. R. Egorova, and A. A. Lamberov

Kazan (Volga Region) Federal University, Kazan, 420008 Russia

e-mail: Giyjaz413@yandex.ru; Segorova@rambler.ru; Alexander.Lamberov@ksu.ru

Received September 9, 2013

Abstract—The formation of silicon oxide structures in the composition of an alumina–chromium catalyst for the dehydrogenation of *iso*-butane is studied by means of nitrogen adsorption, XRD analysis, solid-state ^{29}Si NMR spectroscopy, temperature-programmed desorption of ammonia, and UV-Vis and Raman spectroscopy. It is established that 0.5–1.2 wt % silicon was distributed on the catalyst surface in the form of $Si(OSi)_4$ structures. As the silicon content was increased to 2.2–3.6 wt %, $Si(OSi)_3(O–)$ structural elements were present on the surface in addition to $Si(OSi)_4$. The formation of silicon oxide structures on the catalyst surface was responsible for an increase in the concentration of Cr(III) ions and a decrease in the surface acidity; the activity and selectivity of the catalysts in the reaction of *iso*-butane dehydrogenation increased.

Keywords: alumina–chromium catalyst, silicon, chromium(III) oxide, dehydrogenation

DOI: 10.1134/S2070050414010036

INTRODUCTION

The development of selective catalytic systems that retain their characteristics under high-temperature operating conditions is a problem of considerable current interest in the context of the high-performance processing of hydrocarbon raw materials, which is closely related to the need to reduce power consumption and harmful atmospheric emissions at petroleum chemical plants. For example, a microspherical alumina–chromium catalyst, subjected to short-term action of high temperatures (above 900°C), is used at plants for the fluidized-bed dehydrogenation of C_4–C_5 paraffins into corresponding olefins.

The introduction of additives, modifiers and promoters, for example, zirconium, tin, or phosphorus has been proposed in order to improve the performance characteristics and thermal stability of alumina–chromium dehydrogenation catalysts. The addition of zirconium thus reduces the Lewis acidity of a catalyst; because of this, its selectivity increases [1]. Tin in the amount of 1–3 wt % as an alumina–chromium catalyst component decreases the chromium(VI) content [2]; as a result, catalyst selectivity in the dehydrogenation of propane increases. Khatib et al. [3] studied the effect of phosphorus on the state of chromium in an alumina–chromium catalyst for the oxidative dehydrogenation of lower paraffins. It was found that the introduction of phosphorus reduces the degree of aggregation of chromium compounds and retards the process of their agglomeration; this facilitates the uniform distribution of chromium on the surface of a support and the formation of Cr(III) oxygen compounds in noncrystalline form. As a result, the activity and selectivity of the catalyst in the oxidative dehydrogenation reaction of propane increases.

Improving the properties of alumina–chromium catalysts by modifying them with silicon compounds is widely described in Russian and foreign patents [4–17]. It has been noted that the introduction of 0.1–10% silicon raises not only activity and selectivity [4–17], but also the thermal stability [4, 5, 16, 17] of catalysts. At the same time, the structural characteristics and surface distribution of silicon in a catalyst and its influence on the nature of an active component were not studied in the cited works.

The aim of this work was to study the structure of silicon oxide moieties immobilized on the surface of an alumina–chromium catalyst in a silicon concentration range of 0.5–3.6 wt % and their effect on the surface acidity and nature of the resulting chromium species and the catalytic properties of catalysts in the reaction of *iso*-butane dehydrogenation.

EXPERIMENTAL

Our test materials were microspherical alumina–chromium catalysts with granule sizes of 40 to 200 μm. A monophase boehmite support, prepared by consecutive thermal and hydrothermal treatment of aluminum trihydroxide under industrial conditions [18] in

an autoclave for 3 h at 195°C, was used for the synthesis of catalysts for *iso*-butane dehydrogenation. Silicon was introduced into the catalyst composition via the incipient wetness impregnation of the support with a silicic acid sol. The catalyst was prepared by impregnating the support with an aqueous solution of chromic anhydride and potassium carbonate, followed by drying in a vacuum. The support was placed in the chamber of a rotary vacuum evaporator and outgassed. Aqueous solutions of the precursors of an active component (chromic anhydride) and a promoter (potassium carbonate) were then added at a residual pressure of approximately 30 Torr in volumes corresponding to the incipient wetness impregnation of the support. After impregnation, the catalyst was dried in a vacuum at a residual pressure of 10–30 Torr and then thermally activated. The chromium and potassium contents of the catalyst were 6.2 wt and 0.7 wt %, respectively.

Thermal treatment of the catalyst was performed in a muffle furnace by heating to 800°C at a rate of 4 K/min in an atmosphere of air and then holding at the specified temperature for 1 h.

The silicon content of the catalyst was determined by X-ray fluorescence spectroscopy on a Clever C31 instrument (ELERAN, Russia). Calibration curves were obtained using standard samples of mixtures of aluminum, chromium, silicon, and potassium oxides.

An Autosorb iQ MP analyzer (Quantachrome, United States) was used. S_{sp} was calculated from the surface area of a nitrogen molecule of 0.162 nm^2 and the density of nitrogen in a normal liquid state of 0.808 g/cm^3 to measure the specific surface area (S_{sp}) and pore volume (V_p) from the adsorption–desorption of nitrogen. The accuracy of measuring S_{sp} was ±3%. The adsorption isotherms were obtained at −196°C after outgassing the sample at 500°C to a residual pressure of 0.013 Pa. The porometric volume and pore diameter distributions were calculated from the desorption branch of an isotherm using the standard Barrett–Joyner–Halenda procedure. The accuracy of measurement was ±13%.

The Cr(VI) content was determined as follows: a solution of sulfuric acid and sodium pyrophosphate was added to a weighed portion (0.4–0.6 g) of a catalyst, and the contents were stirred. A solution potassium iodide was then added, and the contents were stirred and held in the dark for 5 min. The liberated free iodine was titrated with a solution of thiosulfate in the presence of starch until the discoloration of the solution.

The X-ray scattering intensity curves were obtained on an upgraded automatic X-ray diffractometer based on a commercial DRON-2 instrument with independent sample rotation and a counter employing long-wave CuK_α radiation with a graphite monochromator. The range of 2θ angles was 5 to 95°. The diffraction patterns were recorded at 30 kV and 15 mA. Annealed copper foil was used as a reference sample to determine the dimensions of crystallites. Identification was conducted by noting the presence of diffraction lines of the crystalline phases of γ-Al_2O_3 (ICSD no. 66559), θ-Al_2O_3 (ICSD no. 82504), δ-Al_2O_3 (ICSD no. 82604), and α-Al_2O_3 (ICSD no 31545) in a spectrum.

The catalyst samples were studied via solid-state ^{29}Si NMR spectroscopy by rotating the samples at a magic angle with a frequency of 5 kHz. The ^{29}Si NMR spectra of catalysts were recorded on an Avance 400 spectrometer (Bruker, Germany) at an operating frequency of 79.5 MHz with a spectral resolution of 48.83 Hz.

The surface acidity of our alumina–chromium catalysts was determined via the temperature-programmed desorption of ammonia (TPD-NH_3) on a flow-type ChemBet Pulsar instrument equipped with a thermal conductivity detector (Quantachrome, United States). The step of adsorption was conducted in a flow of ammonia for 30 min at a temperature of 100°C. After adsorption, physically sorbed ammonia was removed by purging with helium at 100°C for 30 min. The sample was then cooled to room temperature in a flow of helium. Temperature-programmed desorption was performed from room temperature to 700°C at a rate of 10 K/min. The data on the distribution of acid sites based on the TPD of ammonia were calculated following the procedure described in [19].

The Raman spectra were obtained on a Nicolet Almega XR dispersive Raman spectrophotometer (Thermo Fisher Scientific, United States). The test samples were placed on the sample stage of an Olympus BX-51 microscope under an objective with 50-fold magnification. A laser with a wavelength of 532 nm (the second harmonic of Nd-YAG) was used for excitation. The diameter of a focused laser spot on a sample was ~1 μm. The laser power on the sample did not exceed 10 mW. The spectra were measured within a shift range of 100–1100 cm^{-1} with a spectral resolution of 2 cm^{-1}. Each spectrum was obtained by averaging ten exposures of 10 s each.

UV-Vis diffuse reflectance spectra were obtained on a V-650 scanning double-beam spectrophotometer (Jasco, Japan) connected to an ISV-722 integrating sphere (Jasco, Japan) with a diameter of 60 mm covered with $BaSO_4$ inside. A plate of $BaSO_4$ was used as a reference. To measure the spectra, samples of catalyst and chromium(III) oxide 40–100 μm in size were placed into a holder with a quartz window. The spectra were measured in the range of 200–800 nm (12500–50000 cm^{-1}) with a spectral resolution of 2 nm. Data on the diffuse reflectance of the catalyst and chromium(III) oxide samples in the UV-Vis region were interpreted using the Kubelka–Munk function of each wave number.

The carbon content of the catalysts was determined on a HORIBA EMIA-510 instrument (Japan) equipped with a thermal conductivity detector following the ASTM D 3663-99 procedure by combusting

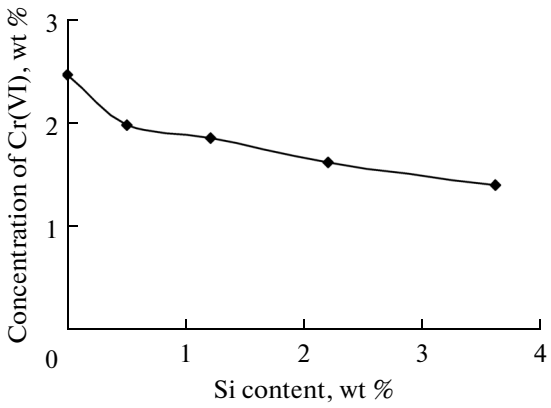

Fig. 1. Dependence of the concentration of Cr(VI) in catalysts on the silicon content.

test catalyst samples of ~1 g in a flow of oxygen at a temperature of 1450°C for 60 s.

Catalysts were tested in the reaction of *iso*-butane dehydrogenation in a fixed-bed flow reactor using an automated laboratory catalytic unit. The operating parameters of the catalytic unit (evaporator and reactor temperatures, gas flow rates, and reactor pressure) were specified and controlled with a program for computer control over the unit. The reactor was loaded with 2 cm^3 of catalyst with a particle size of 40–200 μm. A gaseous mixture containing 30 vol % of an industrial *iso*-butane fraction in argon was used as feed for dehydrogenation. The hourly space velocity of the gas mixture was 1800 h^{-1}. The flow rates of the *iso*-butane fraction, argon, and air were controlled by means of computer-controlled electronic gas flow regulators. The composition of the industrial *iso*-butane fraction was as follows, vol %: *iso*-butane, 99.1; *n*-butane, 0.6; butylenes, 0.2; and propane, 0.1.

The catalyst bed temperature was controlled with the aid of a chromel-alumel thermocouple, and the specified value was maintained with a computer-controlled RPN-4 thermoregulator (ITM, Russia). The temperature was held to within ±1%. Before conducting the dehydrogenation reaction, the catalyst was activated at 650°C in a flow of air at a space velocity of 1800 h^{-1} for 30 min. The duration of dehydrogenation was 130 min. The process temperature was 570°C. For each catalyst sample, three cycles of dehydrogenation were performed by purging with argon for 5 min with subsequent regeneration at 650°C with air at a rate of 1800 h^{-1} for 130 min between each cycle of dehydrogenation. The data from the third cycle of dehydrogenation were taken as the results from our analyses of catalytic activity. After the third cycle of dehydrogenation, the catalyst was no longer subjected to regeneration, and the reactor was cooled to room temperature with a flow of argon. The carbon content of the catalyst unloaded from the reactor was then determined.

The hydrocarbon compositions of the *iso*-butane fraction and contact gas was monitored by means of gas chromatography on a GKh-1000 instrument (Khromos, Russia), which contained a flame-ionization detector and a VP-Alumina/KCl capillary column (VICI Valco, United States). The components were identified by calibrating the chromatograph using standard substances. The relative error in determining the component concentrations was no greater than 10%. The concentrations of H_2 and CH_4 were determined on a GKh-1000 chromatograph (Khromos, Russia) by a thermal conductivity detector using a column loaded with NaX. The relative error in determining the component concentrations was no greater than 10%. The chromatographic analysis data were fed into a computer, where the gas mixture composition was automatically calculated. Based on the results from chromatographic analysis, we calculated

(1) the conversion of *iso*-butane from the formula

$$X = \frac{C^{\text{feed}}_{i\text{-}C_4H_{10}} V^{\text{feed}} - C^{\text{contact gas}}_{i\text{-}C_4H_{10}} V^{\text{contact gas.}}}{C^{\text{feed}}_{i\text{-}C_4H_{10}} V^{\text{feed}}} \times 100, \%, \quad (1)$$

where $C^{\text{feed}}_{i\text{-}C_4H_{10}}$ is the concentration of *iso*-butane in the feed, vol %; $C^{\text{contact gas}}_{i\text{-}C_4H_{10}}$ is the concentration of *iso*-butane in contact gas, vol %; V^{feed} is the space velocity of *iso*-butane feed, cm^3/min; and $V^{\text{contact gas}}$ is the space velocity of contact gas, cm^3/min.

(2) selectivity to *iso*-butylene from the formula

$$S_{i\text{-}C_4H_8} = \frac{C^{\text{contact gas}}_{i\text{-}C_4H_8} V^{\text{contact gas}}}{C^{\text{feed}}_{i\text{-}C_4H_{10}} V^{\text{feed}} - C^{\text{contact gas}}_{i\text{-}C_4H_{10}} V^{\text{contact gas}}} \times 100, \%, \quad (2)$$

where $C_{i\text{-}C_4H_8}$ is the concentration of *iso*-butylene in the contact gas, vol %.

RESULTS AND DISCUSSION

Analysis of Chemical Composition and Pore Structure

According to Cavani et al. [20], Cr(III) and Cr(VI) ions are found on the surface of oxidized alumina–chromium catalyst. Cr(VI) is represented as residual chromium(VI) oxide and aluminum and potassium chromates [20]. Figure 1 shows our data on the Cr(VI) content in the catalysts. A drop in the concentration of Cr(VI) with the concentration of silicon was observed.

Only the signals characteristic of γ-Al_2O_3 were identified in the diffraction patterns of the initial catalyst and catalyst containing 0.5–3.6 wt % silicon (not given in this work). None of the diffraction peaks characteristic of silicon oxide and zeolite structures and crystalline α-Cr_2O_3 were observed.

The introduction of 0.5–3.6 wt % silicon into the catalyst composition had almost no effect on the pore system characteristics: the specific surface area of the catalysts containing silicon varied over a range of 64–

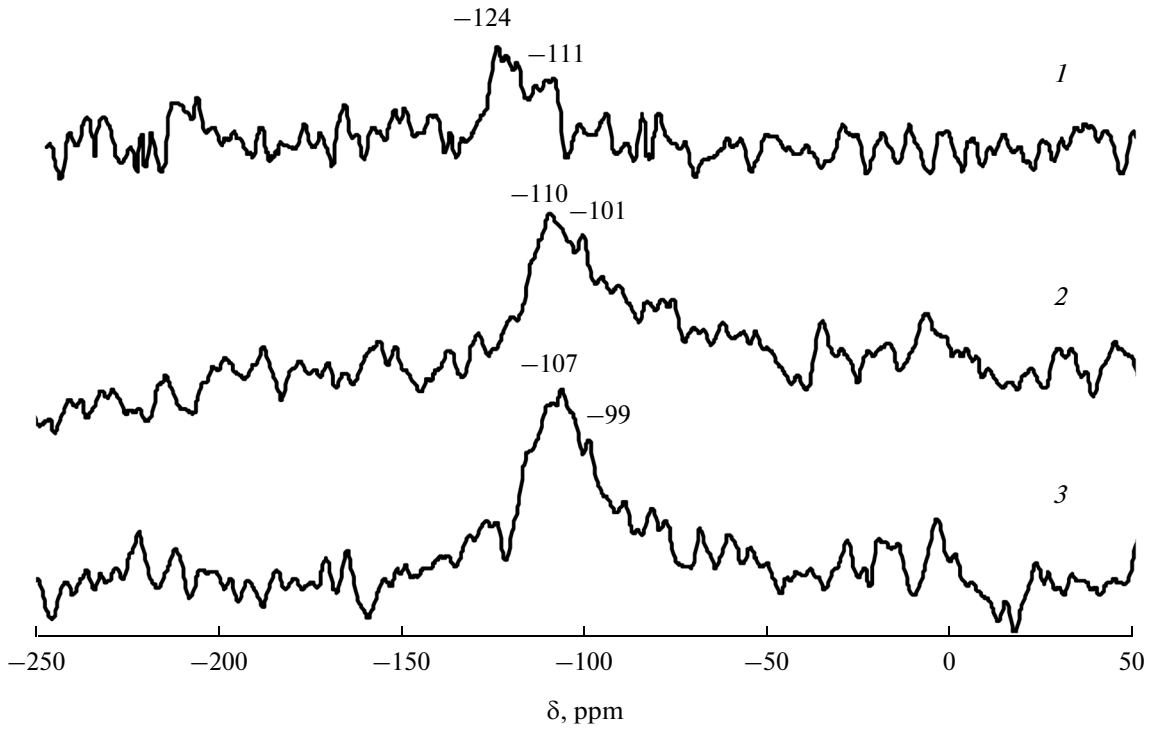

Fig. 2. ^{29}Si NMR spectra of alumina supports with different silicon contents, wt %: (*1*) 1.2, (*2*) 2.2, and (*3*) 3.6.

72 m^2/g, while the porometric volume of the catalysts remained unchanged at 0.22 cm^3/g.

Since there were no transformations in the crystal and pore structures of the catalyst, we may conclude that silicon in the amount of 0.5–3.6 wt % was primarily distributed on the catalyst's surface.

Investigation the Catalysts by ^{29}Si NMR Spectroscopy

To determine the nature of silicon oxide structures in our alumina–chromium catalyst, we analyzed silicon-containing samples by ^{29}Si NMR spectroscopy. The spectra of our alumina–chromium catalysts are shown in Fig. 2. For a catalyst with 0.5 wt %, the ^{29}Si NMR spectra exhibited high noise intensity, while the signals from silicon were difficult to identify; the NMR spectrum of this sample is therefore not presented in this work. The sample containing 1.2 wt % silicon was characterized by a group of low-intensity signals with chemical shifts in the region of −110 to −125 ppm in the ^{29}Si NMR spectra. According to the literature data, these signals correspond to silicon oxide structural elements Q^4 [21–25]. The superscript (in this case, 4) denotes the number of (–OSi) groups surrounding the central atom of silicon [26]. The signals in the NMR spectra with shifts in the region of −110 to −125 ppm thus correspond to $Si(OSi)_4$ elements.

As the silicon concentration in the catalyst was raised to 2.2–3.6 wt %, a shift of resonance signal maxima to the region of −100 to −110 ppm and an increase in their intensity were observed. The signals at −107 to −110 and −99 to −101 ppm in the NMR spectra of samples with 2.2–3.6 wt % silicon correspond to $Si(OSi)_4$ (Q^4) and $Si(OSi)_3(O–)$ (Q^3) structures, respectively [21–25]. The shift of the resonance signals in the NMR spectra into the region of weak fields is indicative of an increase in the degree of silicon coordination with respect to the alumina carrier [23] and free hydroxyl groups [24] as a result of the formation of regions covered with amorphous silicon oxide structures on the catalyst surface and an increase in the area of the catalyst surface occupied by them.

Temperature-Programmed Desorption of Ammonia

The distribution of silicon oxide structures on the surface of an alumina–chromium catalyst changes its characteristics, e.g., the acidic surface properties and state of the active component.

Experiments on the temperature-programmed desorption of ammonia were performed to study the effect silicon has on the surface acidity of catalysts. Figure 3 and Table 1 summarize the data from analyzing the acidic properties of alumina–chromium catalysts.

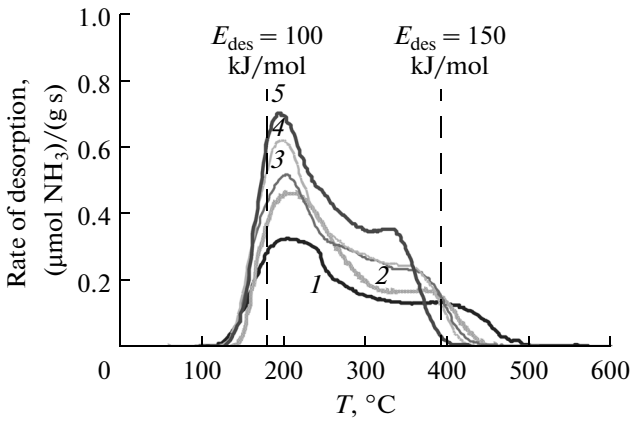

Fig. 3. TPD spectra of ammonia for the samples of alumina–chromium catalysts with different silicon contents, wt %: (*1*) 0, (*2*) 0.5, (*3*) 1.2, (*4*) 2.2, and (*5*) 3.6.

The total concentration of the acid sites of the initial alumina–chromium catalyst was 72.4 μmol/g. The curve of the TPD of ammonia for this sample contained an intense maximum in the low-temperature region (≈190°C) and a wide shoulder in the region of 300–500°C (see Fig. 3). The catalyst's strongest acid sites had an ammonia desorption energy of 170–180 kJ/mol. As a result of introducing 0.5–3.6 wt % silicon into the catalyst's composition, the surface acidity grew to 78.7–109.6 μmol/g (see Table 1) and the distribution of the acid site strengths changed. As the concentration of silicon was raised from 0 to 3.6 wt %, the intensity of low-temperature component of the TPD curves increased as a result of the formation of medium-strength Brønsted and Lewis acid sites [27, 28]. The new Brønsted acid sites were hydroxyl groups bound to silicon atoms [27]. The maximum intensity in the high-temperature region of the TPD spectra also fell to zero upon the introduction of silicon, indicating the disappearance of strong acid sites (see Fig. 3). An analogous effect, was observed in [27, 28], but when silicon was introduced into an alumina support. We assume that as a result of introducing the silicon, the number of tetrahedral vacancies occupied by aluminum atoms diminishes. As is well known, the tetrahedrally coordinated Al(III) ion is a strong Lewis acid site [29].

UV-Vis Spectroscopy

The formation of surface silicon oxide moieties leads to transformations of the active component of a catalyst, which we studied by electronic and molecular spectroscopy.

The UV-Vis spectra of alumina–chromium catalysts contain absorption bands at ≈16900, ≈21750, and ≈27300 cm^{-1} and a shoulder in the region of ≈31000–45000 cm^{-1} (Fig. 4). The bands at ≈16900 and ≈21750 cm^{-1} correspond to *d–d* electron transitions in the $Cr(III)_{oct}$ ions on the catalyst surface [20, 30, 31]. The signal at ≈27300 cm^{-1} and the shoulder in the region of ≈31000–45000 cm^{-1} are due to $^1A_{1g} \rightarrow {}^1T_{2g}$ charge transfer in mono- and polychromates [20, 30, 31].

As the silicon content was raised from 0 to 3.6 wt %, the band at ~27300 cm^{-1} shifted to the short-wave region, and the signal intensity at ~21750 cm^{-1} grew (see Fig. 4). This could indicate a reduction in the symmetry of surface chromates due to an increase in the degree of oligomerization of Cr(VI) compounds as a result of the formation of polychromates [20, 32]. In turn, a monotonic increase in the signal intensity at ≈16900 cm^{-1} with the rise in the concentration of silicon characterizes the increase in the surface concentration of $Cr(III)_{oct}$ [33]. The drop in signal intensity at ≈27300 cm^{-1}, which is characteristic of mono- and polychromates [20], suggests a reduction in the Cr(VI) content.

Table 1. Ammonia TPD data for alumina–chromium catalysts

Silicon content, wt %	Total	Concentration of acid sites, μmol/g (%)		
		including		
		weak	medium	strong
		(E_d < 100)	(100 < E_d < 150)	(E_d > 150)
0	72.4	9.3 (12.9)	53.4 (73.8)	9.6 (13.3)
0.5	78.7	9.0 (11.5)	64.3 (81.6)	5.4 (6.9)
1.2	93.7	12.9 (13.7)	78.0 (83.2)	2.8 (3.0)
2.2	102.8	15.7 (15.3)	85.4 (83.2)	1.6 (1.6)
3.6	109.6	13.8 (12.6)	95.6 (87.2)	0.2 (0.2)

Raman Spectroscopy

The Raman spectra of our alumina–chromium catalysts are presented in Fig. 5. The Raman spectrum of the initial alumina–chromium catalyst indicate the presence of hydrated dichromates on its surface (the Raman signals at 906 and 945 cm^{-1} [34]) and also $Cr(III)_{oct}$, as demonstrated by the weak signal at 564 cm^{-1} [31, 34] (see Fig. 5, spectrum *1*). The introduction of 0.5–1.2 wt % silicon was accompanied by an increase in signal intensity at ≈550 cm^{-1}, a drop in signal intensities at 905 and 948 cm^{-1}, and the appearance of signals characteristic of dehydrated polychromates in the regions of 611, 850–900, and 1000 cm^{-1} [34] (see Fig. 5, spectra *2*, *3*). As the concentration of silicon was raised to 2.2–3.6 wt %, the intensities of the signals of $Cr(III)_{oct}$ at 350 and 550 cm^{-1} [35] grew, and the signals of mono- and polychromates in the region of 800–1000 cm^{-1} diminished [31] (see Fig. 5, spectra *4*, *5*).

The increase in the intensity of signals due to electron transitions in $Cr(III)_{oct}$ in the UV-Vis spectra of the catalyst (see Fig. 4) and the $Cr(III)_{oct}$–O bond vibrations in the Raman spectra (see Fig. 5) upon raising the silicon content of the catalyst indicates an increase in the surface concentration of Cr(III) compounds, probably in the form of chromium(III) oxide clusters [31]. According to UV-Vis and Raman spectroscopy data, introduction of silicon into the catalyst's leads to the preferred formation of surface polychromates, which are converted into oxygen compounds of chromium(III) in the reducing atmosphere of the reaction.

Catalytic Tests

Table 2 summarizes the results from studying catalyst properties. The initial catalyst was characterized by an *iso*-butane conversion of 48.5–48.9% under the conditions of dehydrogenation at 570°C during the first 30–80 min. As the reaction time was increased to 130 min, the catalyst activity in the reactions of both *iso*-butane dehydrogenation and hydrocarbon cracking decreased due to the surface being blocked by carbon deposits.

As a result of introducing 0.5–3.6 wt % silicon into the catalyst, its catalytic properties were improved, and the conversion of *iso*-butane and selectivity to *iso*-butylene increased. The rise in dehydrogenation activity can be explained by modifications of the catalyst surface as a result of the formation of silicon oxide structures. As is known from the literature, a hydrated surface of aluminum oxide has zero charge potential at pH 8.5–9 [36], while the hydrated surface of silicon oxide is much more acidic [37]. On the latter surface, the reaction $2CrO_4^{2-} + 2H^+ \leftrightarrow Cr_2O_7^{2-} + H_2O$ therefore shifts to the formation of di- and polychromates. Consequently, the degree of polymerization of surface

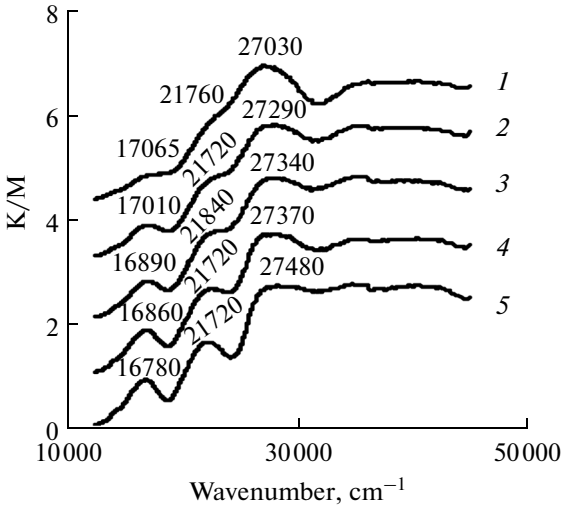

Fig. 4. UV-Vis diffuse reflectance spectra of alumina–chromium catalysts with different silicon contents, wt %: (*1*) 0, (*2*) 0.5, (*3*) 1.2, (*4*) 2.2, and (*5*) 3.6.

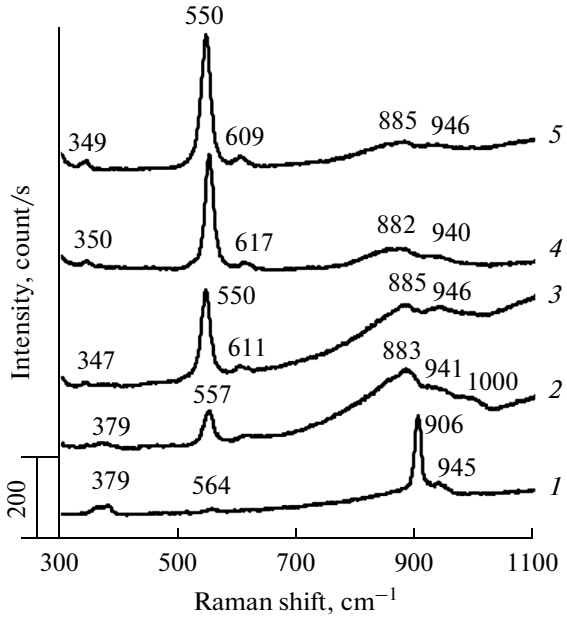

Fig. 5. Raman spectra of alumina–chromium catalysts with different silicon contents, wt %: (*1*) 0, (*2*) 0.5, (*3*) 1.2, (*4*) 2.2, and (*5*) 3.6.

chromates increases upon the formation of silicon oxide moieties, and the number of chromium ions bound to the support's surface through Al–O–Cr and Si–O–Cr bonds decreases. After the thermal activation of the catalyst, a smaller amount of Cr(VI) compounds were stabilized on the support surface (see Fig. 1), and more Cr(III) oxygen compounds were formed (as was confirmed by UV-Vis and Raman spectroscopy, see Figs. 4, 5). Many authors [20, 38–47] attribute the activity of an alumina–chromium catalyst in the dehydrogenation of paraffins to the Cr(III) ions, pos-

Table 2. Results from catalytic tests in the reaction of *iso*-butane dehydrogenation (t_p = 570 °C)

C(Si), wt %	τ, min	Contact gas composition, vol %					*X*, %	$S_{i\text{-}C_4H_8}$, %	*C*, wt %
		H_2	C_1–C_3	C_4H_{10}	C_4H_8	C_{5+}			
0	30	31.6	3.2	34.4	30.8	0	48.5	95.3	0.48
	80	31.9	3.0	34.0	31.1	0	48.9	95.5	
	130	29.9	2.8	37.8	29.3	0	44.9	95.5	
0.5	30	32.7	2.9	32.6	31.8	0	50.6	95.9	0.42
	80	33.2	2.5	32.0	32.2	0.1	51.2	96.4	
	130	30.3	2.4	37.7	29.6	0	45.0	96.3	
1.2	30	33.4	2.5	31.7	32.4	0	51.6	96.3	0.32
	80	34.9	2.2	29.1	33.8	0	54.6	97.0	
	130	32.4	2.2	33.8	31.6	0	49.2	96.7	
2.2	30	34.9	2.2	29.1	33.7	0	54.5	96.9	0.30
	80	35.2	1.9	28.8	34.0	0.1	54.9	97.2	
	130	33.5	1.7	32.3	32.5	0	50.9	97.5	
3.6	30	35.0	2.1	29.0	33.8	0.1	54.6	96.8	0.27
	80	33.7	1.8	31.8	32.7	0	51.4	97.1	
	130	31.7	1.6	35.7	30.9	0	47.1	97.2	

sibly in the form of dispersed chromium(III) oxide [20], also referred to as chromium(III) oxide clusters [31, 43]. Weckhuysen et al. [38] observed a proportional relationship between the concentration of Cr(III) ions detected by in situ UV-Vis spectroscopy and activity in the dehydrogenation of *iso*-butane. It is therefore likely that the dehydrogenation activity of the catalyst grows as a result of an increase in the concentration of Cr(III) ions in the catalyst upon the introduction of 0.5–3.6 wt % silicon.

The transformation of the catalyst's surface area upon the formation of silicon oxide structures was responsible for changes in the acidic properties of the catalyst: as the silicon content was increased from 0 to 3.6 wt %, the strongest acid sites gradually disappeared and the concentration of acid sites characterized by ammonia desorption energies higher than 150 kJ/mol decreased (see Fig. 3 and Table 1) due likely to a reduction in the number of tetrahedrally coordinated aluminum atoms, which are strong Lewis acid sites, in the catalyst. It is well known that the strong acid sites of catalysts based on aluminum oxide participate in the side reactions of hydrocarbon cracking [27]. As a result of the introduction of silicon and an increase in its concentration, a decrease in the rate of hydrocarbon cracking and an increase in selectivity to *iso*-butylene were thus observed during the dehydrogenation of *iso*-butane on catalysts containing silicon (see Table 2).

It is likely that an increase in the concentration of medium-strength acid sites (see Fig. 3 and Table 1) also has a positive effect on the dehydrogenation activity of catalysts. In a heterolytic mechanism, the first step of the process of dehydrogenation is the adsorption of a paraffin molecule at a coordinatively unsaturated Cr(III) ion as a result of donor-acceptor interaction, when the electron pair of the hydrocarbon occupies the free orbital of the Cr(III) ion [48]. In this case, the Cr(III) ion acts as a Lewis acid site, and the higher the adsorption capacity of the catalyst for paraffin molecules, the higher its activity in the dehydrogenation reaction. It was noted in [27, 49] that the medium-strength acid sites play an important role in the adsorption of saturated hydrocarbon molecules. Based on the above, we may conclude that an increase in the concentration of the medium-strength acid sites could enhance the dehydrogenating activity of the catalyst.

The sample with 0.5 wt % silicon exhibited the stability of the dehydrogenation activity in times close to those of the initial catalyst. The conversion of *iso*-butane in its presence thus fell from 51 to 45% as the process time was increased from 80 to 130 min. This behavior of the catalyst over time suggests similar distributions of the active dehydrogenation sites on the surfaces of the initial catalyst and that the catalyst containing 0.5 wt % Si. The dehydrogenating properties of samples with 1.2–2.2 wt % were more stable over time. This could be explained by a lower degree of active site blocking by carbon deposits as a result of the formation of surface silicon oxide structures and a corresponding drop in the concentration of the strong acid sites active in the reactions of hydrocarbon condensation [50].

The catalyst sample containing 3.6 wt % silicon had the greatest surface coverage by silicon oxide elements, as was confirmed by the intensities of signals

corresponding to the silicon oxide elements Q^3 and Q^4 in the NMR spectrum (see Fig. 2, spectrum *3*). The greatest surface concentration of Cr(III) ions, presumably in the form of chromium(III) oxide clusters [31, 43], was thus noted in this catalyst (see Figs. 4, 5, spectrum *5*), and was probably responsible for the high activity of the catalyst in the first minutes of the dehydrogenation process. However, the conversion of *iso*-butane diminished along with the time of dehydrogenation (see Table 2). The absence of an induction period on the catalyst with 3.6 wt % silicon can be explained by the minimal Cr(VI) content of all investigated samples. It is likely that in this catalyst, the effect of the blocking of the active dehydrogenation sites by high-molecular-weight carbon deposits on the activity had grew as the process time increased, relative to the effect of the transformation of Cr(VI) compounds to an active phase of chromium(III) ions.

The yield of C_1–C_3 hydrocarbons on the catalyst containing 3.6 wt % silicon was the lowest in the investigated series. This could be explained by the disappearance of the strongest acid sites and the minimal concentration of acid sites with ammonia desorption energies greater than 150 kJ/mol (see Fig. 3, Table 1), due to the greater surface coverage by silicon oxide structures and the corresponding reduction in the surface concentration of the Lewis acid sites of aluminum oxide.

CONCLUSIONS

We studied the effect of surface silicon oxide structures formed upon introducing 0.5–3.6 wt % silicon on the properties of alumina–chromium catalyst for the dehydrogenation of *iso*-butane, e.g., its surface acid properties and the state of the active component.

Upon the introduction of 0.5–3.6 wt % silicon, the Cr(VI) content of the catalyst diminished; at the same time, its crystal and pore structures remained almost unchanged, along with the specific surface areas and pore volumes of the initial catalyst and the catalyst containing silicon.

In the catalyst with 0.5–1.2 wt % silicon, silicon was distributed over the surface in the form of $Si(OSi)_4$ structural elements. According to ^{29}Si NMR spectroscopy data, the degree of coordination of silicon oxide particles with respect to the surface of aluminum oxide and free hydroxyl groups grew as the silicon content was raised to 2.2–3.6 wt % as a result of the increased distribution of these particles and their amorphization.

The formation of the oxygen compounds of silicon transforms the state of the active component, i.e., raises the surface concentration of Cr(III) ions. The surface acidity simultaneously increases due to the formation of medium-strength Lewis and Brønsted acid sites. The disappearance of strong acid sites as a result of a drop in the number of tetrahedrally coordinated aluminum atoms that are strong Lewis acid sites is also observed.

The surface transformation of alumina–chromium catalyst upon the introduction of silicon leads to changes in its catalytic properties. It is likely that the dehydrogenating activity of the catalysts increases as a result of growth in the surface concentration of Cr(III) compounds, presumably in the form of chromium(III) oxide clusters [31, 43]. At the same time, the concentration of strong acid sites, and thus the yield of hydrocarbon cracking products, diminishes.

ACKNOWLEDGMENTS

This work was supported by the RF Ministry of Education and Science.

REFERENCES

1. Korhonen, S. Airaksinen, S., et al., *Appl. Catal. A*, 2007, vol. 333, p. 30.
2. Cabrera, F. Ardissone, D., et al., *Catal. Today*, 2008, vols. 133–135, p. 800.
3. Khatib, S.J. Fierro, J.L.G., et al., *Top. Catal.*, 2009, vol. 52, p. 1459.
4. RF Patent 2200143, 2003.
5. RF Patent 2148430, 2000.
6. RF Patent 2156233, 2000.
7. RF Patent 2127242, 1999.
8. RF Patent 2287366, 2006.
9. RF Patent 2167709, 2001.
10. RF Patent 2176157, 2001.
11. RF Patent 2160634, 2000.
12. RF Patent 97113451, 1999.
13. RF Patent 677194, 2001.
14. EEC Patent 637578, 1995.
15. Jpn. Patent 7010350, 1995.
16. US Patent 4746643, 1988.
17. US Patent 6362385, 2002.
18. Egorova, S.R. Kataev, A.N., et al., *Katal. Prom-st.*, 2009, no. 6, p. 48.
19. Yushchenko, V.V., *Zh. Fiz. Khim.*, 1997, vol. 71, no. 4, p. 628.
20. Cavani, F. Koutyrev, M., et al., *J. Catal.*, 1996, vol. 158, p. 236.
21. Oka, H. and Ohki. H., *Anal. Sci.*, 2010, vol. 26, p. 411.
22. Sato, S., Sodesawa, T., et al., *J. Mol. Catal.,* 1991, vol. 66, p. 343.
23. Lippmaa E., Magi M., et al., *J. Am. Chem. Soc.*, 1981, vol. 103, p. 4992.
24. Lindblad, M. and Root, A., Abstract of Papers, in *Preparation of Catalysts VII. Proc. 7th Int. Symp. "Scientific Bases for the Preparation of Heterogeneous Catalysts"*, Amsterdam: Elsevier, vol. 118, 817.
25. McMillan, M. Brinen, J.S., et al., Colloids Surf., 1989, no. 38, p. 133.

26. Engelhardt, G. and Michel, D., *High Resolution Solid-State NMR of Silicates and Zeolites*, Chichester: John Wiley, p. 485.
27. Iengo, P., Di Serio, M., et al., *Appl. Catal. A*, 1998, no. 170, p. 225.
28. Finocchio E., Busca, G., et al., *Catal. Today*, 1997, no. 33, p. 335.
29. Paukshtis, E.A., *Infrakrasnaya spektroskopiya v geterogennom kislotno-osnovnom katalize* (Infrared Spectroscopy in Heterogeneous Acid-Base Catalysis), Novosibirsk: Nauka, 1992.
30. Sviridov, D.T., Sviridova, R.K., and Smirnov, Yu.F., *Opticheskie spektry ionov perekhodnykh metallov* (Optical Spectra of Transition Metal Ions), Moscow: Nauka, 1976.
31. Weckhuysen, B.M. Wachs, I.E., et al., *Chem. Rev.*, 1996, vol. 96, p. 3327.
32. Zaki, M.I. Fouad, N.E., et al., *Appl. Catal.*, 1986, vol. 21, p. 359.
33. Weckhuysen, B.M. Verberckmoes, An.A., et al., *J. Catal.,* 1997, vol. 166, p. 160.
34. Mentasty, L.R. Gorriz, O.F., et al., *Ind. Eng. Chem. Res.,* 1999, vol. 38, p. 396.
35. Mougin, J., Le Bihan, T., et al., *J. Phys. Chem. Solids*, 2001, vol. 62, p. 553.
36. Stiles, A.B., Catalyst *Supports and Supported Catalysts: Theoretical and Applied Concepts*, Stoneham: Butterworth, 1987.
37. Weckhuysen, B.M., Schoofs, B., and Schoonheydt, R.A., *J. Chem. Soc., Faraday Trans.*, 1997, vol. 93, no. 11, p. 2117.
38. Weckhuysen, B.M. Verberckmoes, A.A., et al., *J. Mol. Catal. A: Chem.*, 2000, vol. 151, p. 115.
39. Airaksinen, S.M.K. Krause, A.O.I., et al., *Phys. Chem. Chem. Phys.*, 2003, vol. 5, p. 4371.
40. Grunert, W. Saffert, W., et al., *J. Catal.*, 1986, vol. 99, p. 149.
41. Hakuli, A. Kytokivi, A., et al., *J. Catal.*, 1996, vol. 161, p. 393.
42. Hakuli, A. Kytokivi, A., et al., *Appl. Catal. A*, 2000, vol. 190, p. 219.
43. Hakuli, A. Harlin, M.E., et al., *J. Catal.*, 1999, vol. 184, p. 349.
44. De Rossi, S., Casaletto et. al., *Appl. Catal. A,* 1998, vol. 167, p. 257.
45. Puurunen, R.L. Weckhuysen, B.M., et al., *J. Catal.*, 2002, vol. 210, p. 418.
46. Carra, S., Ugo, R., Zanderighi, L., *Inorg., Chim. Acta, Rev.*, 1969, vol. 3, p. 55.
47. Puurunen, R.L., Airaksinen, S.M.K., and Krause, A.O.I., *J. Catal.*, 2003, vol. 213, p. 281.
48. Petrov, I.Ya. and Tryasunov, B.G., *Zh. Neorg. Khim.*, 1996, vol. 35, no. 5, p. 1347.
49. Rombi, E., Cutrufello, M.G., et al., *Appl. Catal. A*, 2003, vol. 251, p. 255.
50. Buyanov, R.A., *Zakoksovanie katalizatorov* (Carbonization of Catalysts), Novosibirsk: Nauka, 1983.

Translated by V. Makhlyarchuk